New Alternating D–A_1–D–A_2 Copolymer Containing Two Electron-Deficient Moieties Based on Benzothiadiazole and 9-(2-Octyldodecyl)-8*H*-pyrrolo[3,4-*b*]bisthieno[2,3-*f*:3′,2′-*h*] quinoxaline-8,10(9*H*)-dione for Efficient Polymer Solar Cells

M. L. Keshtov,[1] S. A. Kuklin,[1] D. Y. Godovsky,[1] A. R. Khokhlov,[1,2] R. Kurchania,[3] F. C. Chen,[4] Emmanuel N. Koukaras,[5,6] G. D. Sharma[7]

[1]A.N. Nesmeyanov Institute of Organoelement Compounds, Russian Academy of Sciences, Vavilova str., 28, Moscow, 119991, Russia
[2]Faculty of Physics, Lomonosov Moscow State University, 1-2 Leninskiye Gory, Moscow, 119991, Russian Federation
[3]Department of Physics, Maulana Azad National Institute of Technology (MANIT), Bhopal, Madhya Pradesh, 462051, India
[4]Department of Photonics, National Chiao Tung University, 1001 University Road, Hsinchu, 30010, Taiwan
[5]Institute of Chemical Engineering Sciences, Foundation for Research & Technology, Hellas, Stadiou Str. Platani, Patras, 26504, Greece
[6]Molecular Engineering Laboratory, Department of Physics, University of Patras, Patras, 26500 GR, Greece
[7]R&D Center for Engineering and Science, JEC Group of Colleges, Jaipur Engineering College, Jaipur, Rajasthan 303101, India
Correspondence to: M. L. Keshtov (E-mail: keshtov@ineos.ac.ru) or G. D. Sharma (E-mail: sharamgd_in@yahoo.com; gdsharma273@gmail.com)

Received 16 May 2015; accepted 16 July 2015; published online 11 August 2015
DOI: 10.1002/pola.27786

ABSTRACT: A novel D–A_1–D–A_2 copolymer denoted as **P1** containing two electron withdrawing units based on benzothiadiazole (BT) and 9-(2-octyldodecyl)−8H-pyrrolo[3,4-b] bisthieno[2,3-f:3′,2′-h]quinoxaline-8,10(9H)–dione (PTQD) units was synthesized and characterized. The resulting copolymer exhibits a broad-absorption spectrum, relatively deep lying HOMO energy level (−5.44 eV) and narrow optical bandgap (1.50 eV). Bulk heterojunction (BHJ) polymer solar cells (PSCs) based on **P1** as donor and $PC_{71}BM$ as acceptor with optimized donor to acceptor weight ratio of 1:2 and processed with DIO/CB solvent showed good photovoltaic performance with power conversion efficiency of 6.21% which is higher than that of the device processed without solvent additive (4.40%). The absorption and morphology investigations of the active layers indicated that structural and morphological changes were induced by the solvent additive. This higher power conversion efficiency could be mainly attributed to the absorption enhancement and improved charge transported in the active layer induced by the better nanoscale morphology of the active layer. This study demonstrated that a copolymer with two different acceptor moieties in the backbone may be promising candidate as donor copolymer for solution processed BHJ PSCs. © 2015 Wiley Periodicals, Inc. J. Polym. Sci., Part A: Polym. Chem. **2016**, *54*, 155–168

KEYWORDS: bulk heterojunction; charge transport; copolymers based on strong and weak acceptors; polymer solar cells; solvent additives

INTRODUCTION Polymer solar cells (PSCs) based on the bulk heterojunction (BHJ) active layer consists of conjugated polymers as donor and fullerene derivatives as acceptor have received lot of attention as energy conversion technology, due to their compatibility with fabricating large-area, flexible, and low cost devices via roll-to-roll processing techniques.[1] Synthesis of new narrow band gap conjugated polymers based on strong and weak acceptors with strong and broad absorption, suitable energy levels, and high charge carrier mobility is the key feature which allows PSC to become a reliable source of energy in the near future.[2] Over the past decade the continuous efforts have been devoted to PSCs development and impressive power conversion efficiency (PCE) values in the range of 8%–10% were achieved.[3,4] This progress has been achieved not only through a better understanding and control of the generation and transport of charge carriers, but also due to the development of a wide range of new narrow-band π-conjugated polymers.[5] However, more accurate models explicitly developed for polymer:fullerene BHJ solar cells have predicted maximum PCEs around

Additional Supporting Information may be found in the online version of this article.

15%[6] and 21%[7] for single BHJ active layer and tandem solar cells, respectively.

One of the methods for the synthesis of narrow bandgap conjugated polymers with low-lying HOMO is a donor–acceptor (D–A) strategy with strict alternation of the donor (D) and acceptor (A) fragments in the main chains of macromolecules.[8] The push–pull effect of donor and the acceptor segments in this design will result in an intra- and/or intermolecular charge transfer (ICT), leading to broader absorption profile and narrower bandgap.[9] Until now many attempts were undertaken to design and synthesize of D–A polymers which exhibit sufficiently high performance when used as donors in the PSC[10] and only a limited number of donor or acceptor building blocks for PSCs have shown high photovoltaic performance.[11] Another alternative molecular strategy was adopted recently to design the ternary copolymers comprises of an additional donor or acceptor unit with appropriate molar ratio into the D–A type copolymer backbone.[12,13] It has been found that the introduction of two electron-acceptor moieties with different absorption pattern into the D–A_1–D–A_2 repeating unit of the copolymer leads to a wider range and higher absorption characteristics of PSCs, in comparison with conventional D–A polymers which contain one donor and one acceptor fragments in the repeating unit of the macromolecule. This approach gives new way to design of new narrow band gap polymers with a wider range of effective absorption of PSCs.[14] More recently, Wang et al. have shown the benefits of D–A_1–D–A_2 strategy, compared with conventional D–A polymers.[15] The performance of this copolymer was greater than D–A_1 and D–A_2 polymers. Moreover, it was shown that alternating copolymer based on the D–A_1–D–A_2 acceptor fragment having regio-regular structure forms π-stacking structure and hence provides higher carrier mobility compared with a random copolymer with two acceptor units.[15]

Encouraged by strategy of two different acceptors in the main backbone of conjugated copolymers, we have prepared a copolymer structure of D–A_1–D–A_2 by introducing two electron-acceptor structures in the elementary unit of the polymer. The 9-(2-octyldodecyl)-8*H*-pyrrolo[3,4-*b*]bisthieno[2,3-*f*:3′,2′-*h*] quinoxaline-8,10(9*H*)-dione (PTQD) monomer containing fused thiophene fragments is an interesting building block due to its quinoid character of π-conjugation, coplanarity of structure, and high electron-withdrawing effect of imide fragment. The fused ring system can maximize the π-orbital overlap by restricting intramolecular rotation in the polymer and possibly to induce face–face π-stacking facilitating charge transport through intermolecular hopping. On the other hand the fused ring can make the polymer backbone more rigid and coplanar therefore enhancing effective π-conjugation lowering band gap and extending absorption. Moreover, 4,7-di(thiophen-2-yl)-2,1,3-benzothiadiazole (DTBT) is very commonly used as the electron withdrawing unit in donor–acceptor based small molecules and polymers for both OPV and OFET applications.[16]

In this study, alternating D–A_1–D–A_2 copolymer **P1** was synthesized and characterized as comprising the thiophene as a donor and two electron acceptor moities: benzothiadiazole (BT) and 9-(2-octyldodecyl)-8H-pyrrolo[3,4-b]bisthieno [2,3-f:3′,2′-h] quinoxaline-8,10(9H)-dione (PTQD) as acceptors in the repeating unit. The targeted copolymer, named as **P1**, was obtained using a Pd-catalyzed Stille coupling reaction between PTQD and 4,7-di(thiophen-2-yl)-2,1,3-benzothiadiazole unit BTDA. The resulting copolymer showed a good thermal stability and a deep HOMO energy level of −5.44 eV, and a broad absorption spectrum (350–800 nm). The optimized PSCs using **P1** as donor and [6,6]-phenyl C_{71}-butyric acid methyl ester ($PC_{71}BM$) as acceptor showed a PCE of 6.21% with a high V_{oc} of 0.84 V, J_{sc} of 11.74 mA/cm^2, and FF of 0.63, under stimulated illumination of AM1.5G, 100 mW/cm^2.

EXPERIMENTAL

Instruments

The ^{1}H and ^{13}C NMR (nuclear magnetic resonance) spectra were recorded on a Bruker Avance-400 spectrometer at a frequency of 400.13 and 100.62 MHz, respectively. UV–vis (ultraviolet–visible) absorption was tested on a Shimadzu UV-3600 UV–vis-NIR spectrometer. The bandgap was calculated according to the onset absorption of UV–vis spectrum ($E_g = 1240/\lambda_{onset}$, eV). Molecular weight and dispersity of copolymer were analyzed by gel permeation chromatography (GPC), conducted on a PL-GPC 220 system using polystyrene as standard and 1,2,4-trichlorobenzene as eluent at 150 °C. Thermogravimetric analysis (TGA) measurements were carried out with Perkin–Elmer TGA-7 at a heating rate of 10 °C/min under nitrogen. Cyclic voltammetry (CV) of polymer films was performed on a CHI660a electrochemical analyzer with a three-electrode cell at a scan rate of 100 mV/s (glassy carbon electrode, Pt wire and saturated calomel electrode), respectively. Bu_4NClO_4 (0.1 mol/L) was used as electrolyte and anhydrous acetonitrile (drying with CaH_2) was used as the solvent. The potentials were measured against the Ag/Ag^+ (0.01 M $AgNO_3$) reference electrode; ferrocene/ferrocenium ion (Fc/Fc^+) was used as internal standard (0.32 V). Energy of HOMO and LUMO levels were calculated according to eqs 1 and 2, and electrochemically determined bandgaps were deduced from the difference between onset potentials from oxidation and reduction of copolymers as depicted in eq 3

$$E_{HOMO} = -(E^{ox}{}_{onset} + 4.48)\ (eV) \quad (1)$$

$$E_{LUMO} = -\left(E^{red}{}_{onset} + 4.48\right)\ (eV) \quad (2)$$

$$E_g{}^{ech} = E_{HOMO} - E_{LUMO}(eV) \quad (3)$$

The morphologies of the copolymer/$PC_{71}BM$ blend films were investigated by a SPI 3800N atomic force microscope (AFM) in contacting mode with a 3 μm scanner.

Materials

All reagent, unless otherwise specified, were obtained from Aldrich and Acros and used as received. All the solvents were freshly distilled prior to use.

Synthesis of Monomer PTQD and Polymer PI

5,6-Dichloropyrazine-2,3-dicarboxylic acid anhydride (1) was prepared according to the reported procedure.[17] Yield was 78%, m.p. 260–261 °C, lit. 250–252 °C.

2-Octyldodecylamine was prepared according to the literature method.[18] Yield was 85%. ^{1}H NMR (400.13 MHz; $CDCl_3$; δ, ppm): 2.61 (d, 2H); 1.4–1.2 (m, 35H); 0.89 (t, 6H).

2-Octyldodecylamine hydrochloride (2): The solution of 2-octyldodecylamine (8 g, 26.884 mmol) in dry THF (400 mL) was purged with dry HCl for 1 h. Reaction mixture was evaporated and dried *in vacuo*. Product was used without further purification. Yield is 8.5 g (94.7%). ^{1}H NMR (400.13 MHz; dmso-d6; ppm): 8.02 (br.s, 3H); 2.64–2.65 (m, 2H); 1.6 (m, 1H); 1.4–1.2 (m, 34H); 0.85 (t, 6H).

5,6-Dichloropyrazine-2,3-dicarboxylic acid N-(2-octyldodecyl)amide (3) was prepared by the modified literature method. To the mixture of 5,6-dichloropyrazine-2,3-dicarboxylic acid anhydride (**1**) (8.48 g, 38.72 mmol) and 2-octyldodecylamine hydrochloride (**2**) (19.4 g, 58.08 mmol) acetic anhydride (20 mL) was added, and reaction mixture was heated at 135 °C for 1 h. Water (200 mL) was added, and the mixture was extracted with toluene (3 × 100 mL). Organic extract was washed with water, dried with $MgSO_4$, filtered, and evaporated. Yield was 17.95 g (93%). ^{1}H NMR (400.13 MHz; $CDCl_3$; δ, ppm): 3.71 (d, 2H); 1.8 (m, 1H); 1.4–1.2 (m, 32H), 0.89 (t, 6H). 13C NMR (125 MHz; $CDCl_3$; δ, ppm): 162.46; 153.51; 143.55; 43.24; 37.09; 31.92; 31.08; 31.35; 29.93; 29.63; 29.58; 29.53; 29.35; 26.15; 22.70; 22.68; 14.13.

6-(2-Octyldodecyl)-2,3-di(thiophen-2-yl)- 5*H*-pyrrolo[3,4-*b*]pyrazine-5,7(6*H*)-dione (4): The mixture of 5,6-dichloropyrazine-2,3-dicarboxylic acid N-(2-octyldodecyl)amide (**3**) (8.91 g, 17.86 mmol), 2-(tributylstannyl)thiophene (16 g, 42.86 mmol), $Pd(PPh_3)_4$ (1 g, 0.865 mmol) in dry THF (400 mL) was refluxed for 65 h under argon. After cooling the mixture was evaporated and dried. Title compound was obtained by column chromatography on SiO_2 (hexane:toluene = 1:1). Yield was 8.3 g (78%) of yellow solid. ^{1}H NMR (400.13 MHz; $CDCl_3$; δ, ppm): 7.60 (m, 2H); 7.50 (m, 2H); 7.07 (m, 2H); 3.73 (d, 2H); 1.4–1.2 (m, 33H); 0.89 (t, 6H). ^{13}C NMR (125 MHz; $CDCl_3$; δ, ppm): 164.37; 150.59; 143.14; 139.69; 131.21; 130.70; 127.94; 42.83; 37.11; 31.92; 31.90; 29.97; 29.65; 29.64; 29.62; 29.36; 29.31; 26.25; 22.70; 14.14.

6-(2-Octyldodecyl)-2,3-bis(5-bromothiophen-2-yl)-5*H*-pyrrolo[3,4-*b*]pyrazine-5,7(6*H*)-dione (5): To the solution of 6-(2-octyldodecyl)-2,3-di(thiophen-2-yl)-5*H*-pyrrolo[3,4-*b*]pyrazine-5,7(6*H*)-dione (**4**) (8.154 g, 13.75 mmol) in $CHCl_3$ (100 mL) and AcOH (100 mL) NBS (5.34 g; 30 mmol) was added and the mixture was stirred at room temperature for 48 h. Water was added (400 mL), mixture was neutralized with $NaHCO_3$, and extracted with $CHCl_3$. Combined organic phase was dried with $MgSO_4$ and evaporated. Residue was crystallized from CH_2Cl_2–hexane to give 8.5 g (82%) of the title compound. ^{1}H NMR (400.13 MHz; $CDCl_3$; δ, ppm): 7.38 (d, 2H); 7.06 (d, 2H); 3.72 (d, 2H); 1.8 (m, 1H); 1.4–1.2 (m, 32H); 0.89 (t, 6H). ^{13}C NMR (125 MHz; $CDCl_3$; δ, ppm): 173.06; 163.97; 148.85; 143.19; 140.77; 131.05; 130.98; 119.55; 42.91; 37.10; 31.91; 31.38; 29.55; 29.95; 29.63; 29.35; 29.30; 28.70; 26.21; 22.68; 14.13.

2,5-Dibromo-9-(2-octyldodecyl)-8*H*-pyrrolo[3,4-*b*]bisthieno[2,3-*f*:3′,2′-*h*]quinoxaline-8,10(9*H*)-dione (PTQD): The mixture of 6-(2-octyldodecyl)-2,3-bis(5-bromothiophen-2-yl)-5*H*-pyrrolo[3,4-*b*]pyrazine-5,7(6*H*)-dione (**5**) (1 g, 1.33 mmol), iodine (169 mg, 0.665 mmol) in dry toluene (250 mL) was irradiated with medium pressure mercury lamp for 10 h. When reaction mixture was evaporated, residue was washed with acetone, dried, and purified by column chromatography on SiO_2 (toluene as eluent) to give 0.65 g (65%) of the title compound **6**. ^{1}H NMR (400.13 MHz; $CDCl_3$; δ, ppm): 7.71 (s, 2H); 3.83 (d, 2H); 2.01 (m, 1H); 1.2–1.4 (m, 32H), 0.88 (t, 6H). ^{13}C NMR (125 MHz; $CDCl_3$; δ, ppm): 164.25; 143.55; 138.94; 137.27; 136.83; 125.60; 123.06; 43.10; 37.18; 31.92; 31.48; 29.97; 29.64; 29.36; 29.31; 26.27; 22.68; 14.12. Anal. calculated (%) for $C_{34}H_{43}Br_2N_3O_2S_2$: C, 54.47; H, 5.78; N, 5.61; S,8.55. Found: C, 54.35; H, 5.87; N, 5.57; S, 8.51.

Polymer P1

A mixture of 0.6260 g (1 mmol) of 4,7-bis[5-(trimethylstannyl)thiophen-2-yl]-2,1,3-benzothiadiazole (BDTA), 0.7497 g (1 mmol) of 2,5-dibromo-9-(2-octyldodecyl)-8*H*-pyrrolo[3,4-*b*]bisthieno[2,3-*f*:3′,2′–*h*]quinoxaline-8,10(9*H*)-dione (PTQD), and 0.065 g (0.056 mmol) $Pd(Ph_3P)_4$ was placed in a 50 mL three-necked flask equipped with a reflux condenser and magnetic stirrer, and 32 mL of dry toluene was added. The reaction mixture was stirred at 110 °C for 48 h under argon. The mixture was then cooled to room temperature and poured in 200 mL of methanol and filtered. The copolymer was dissolved in chloroform and re-precipitated with methanol, then purified by extraction with methanol, hexane, acetone in a Soxhlet apparatus, and dried in vacuum. Yield was 71%. ^{1}H NMR (400 MHz, $CDCl_3$, δ, ppm): 8.06–7.46 (m, 8H), 4.32 (m, 2H), 2.50–0.40 (m, 39H). Anal. calculated (%) for $(C_{48}H_{49}B_5O_2S_5)_n$: C, 64.90; H, 5.56; N, 7.88; S, 18.05. Found: C, 64.77; H, 5.50; N, 7.53; S, 17.99.

Device Fabrication and Characterization

The BHJ organic solar cells were fabricated using the glass/ITO/PEDOT:PSS/ **P1**:$PC_{71}BM$/Al device architecture. The indium tin oxide (ITO) patterned substrates were cleaned by ultrasonic treatment in aqueous detergent, deionized water, isopropyl alcohol, and acetone sequentially, and finally dried under ambient conditions. The anode consisted of glass substrates patterned with ITO, modified by spin coating with a PEDOT:PSS layer (60 nm) as hole transport and heated for 10 min at 100 °C. Mixtures of **P1** with $PC_{71}BM$ with weight ratios of 1:05, 1:1, and 1:2 and 1:2.5 in chlorobenzene (CB) were prepared and then spin-cast onto the PEDOT:PSS layer and dried overnight at ambient atmosphere at 40 °C. For the **P1**:$PC_{71}BM$ blend processed from 3 vol % of DIO in CB solvent mixture only the 1:2 weight ratio mixture was used. The total concentration of the **P1**:$PC_{71}BM$ was kept constant,

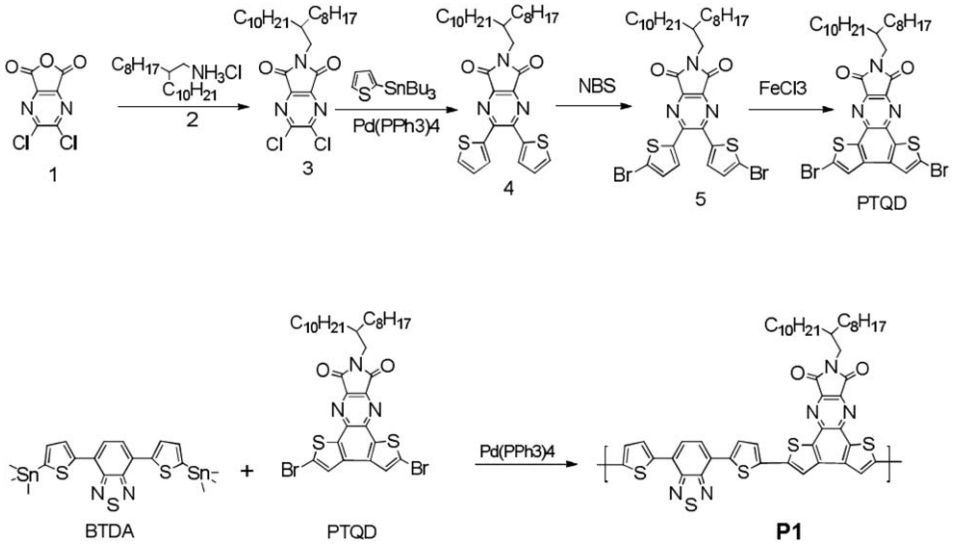

SCHEME 1 Synthetic route for the synthesis of monomer **PTQD** and copolymer **P1.**

that is, 15 mg/mL. The approximate thickness of the active layer was 90 ± 5 nm. Finally, the aluminum (Al) top electrode was thermally deposited on the active layer at a vacuum of 10^{-5} Torr through a shadow mask of area of 20 mm^2. All devices were fabricated and tested in ambient atmosphere without encapsulation. The hole-only and electron-only devices with ITO/PEDOT:PSS/ **P1**:$PC_{71}BM$/Au and ITO/Al/**P1**:$PC_{71}BM$/Al architectures were also fabricated in an analogous way, in order to measure the hole and electron mobility, respectively.

The current–voltage (*J–V*) characteristics of the BHJ organic solar cells were measured using a computer controlled Keithley 238 source meter in dark as well as under simulated AM1.5G illumination of 100 mW/cm^2. A xenon light source coupled with optical filter was used to give the stimulated irradiance at the surface of the devices. The incident photon to current efficiency (IPCE) of the devices was measured illuminating the device through the light source and monochromator and the resulting current was measured using a Keithley electrometer under short circuit condition.

RESULTS AND DISCUSSION

Synthesis and Characterization

In order to obtain new π-conjugated polymer **P1** we have synthesized 2,5-dibromo-9-(2-octyldodecyl)-8*H*-pyrrolo[3,4-*b*] bisthieno[2,3-*f*:3′,2′-*h*]quinoxaline-8,10(9*H*)-dione (**PTQD**). In order to make it 5,6-dichloropyrazine-2,3-dicarboxylic acid anhydride (**1**) was introduced into imidization reaction with octyldodecylamine hydrochloride in the presence of acetic anhydride, and so obtained 5,6-dichloropyrazine-2,3-dicarboxylic acid *N*-(2-octyldodecyl)amide (**3**) interacted with two molar excess of 2-(tributylstannyl)thiophene under the Stille reaction conditions with the formation of intermediate compound 6-(2-octyldodecyl)-2,3-di(thiophen-2-yl)-5*H*-pyrrolo[3,4-*b*]pyrazine-5,7(6*H*)-dione (**4**) with the yield of 73%. The treatment of the latter with *N*-bromosuccinimide (NBS) and following cyclization of intermediate compound 6-(2-octyldodecyl)-2,3-bis(5-bromothiophen-2-yl)-5*H*-pyrrolo[3,4-*b*]pyrazine-5,7(6*H*)-dione (**5**) by $FeCl_3$ lead to the target monomer **PTQD** with the yield as high as 65%. The synthetic route of **PTQD** is shown in Scheme 1. Monomer **PTQD** was thoroughly purified by column chromatography (toluene as eluent) and then recrystallized in order to provide necessary purity for polymerization.

Composition and the structure of intermediate compounds as well as of the target monomer **PTQD** were confirmed by elemental analysis data, ^{13}C NMR and ^{1}H NMR spectroscopy. In particular in the ^{1}H NMR spectrum of monomer **PTQD** in the region of 7.71 ppm one singlet is observed, related to the protons of thiophene fragments [Fig. 1(a)]. In the strong field area at 3.83 and 0.88 ppm one doublet and one triplet are present, related to CH_2 group which is directly connected to the nitrogen atom of imide group and CH_3 groups correspondingly. In the range of 2.2–1.2 ppm one observes the multiplets, related to the retaining atoms of hydrogen of alkyl group. The ratio of integral intensities of aromatic part to aliphatic fully corresponds to the proposed structure of **PTQD**. In ^{13}C NMR spectrum of **PTQD** in weak field area seven peaks are present which are related to seven aromatic atoms of carbon, and in strong field area at 14.12 and 43.10 ppm correspondingly the signals appear, typical for terminal CH_3 and CH_2 groups, which are directly bounded to nitrogen atom correspondingly, and in the range of 37.18–22.68 ppm one finds the signals, related to the rest of aliphatic atoms of carbon, which is in accordance with the proposed structure [Fig. 1(b)].

The synthetic route of the copolymer **P1** is shown in Scheme 1. The synthesis of copolymer **P1** was carried out in the boiling toluene during 48 h under Stille reaction conditions. The composition and chemical structure of polymer **P1** was determined by elemental analysis and ^{1}H NMR (Fig. 2). The process was carried out in the homogeneous conditions and allowed to obtain polymer as a deep violet powder with the

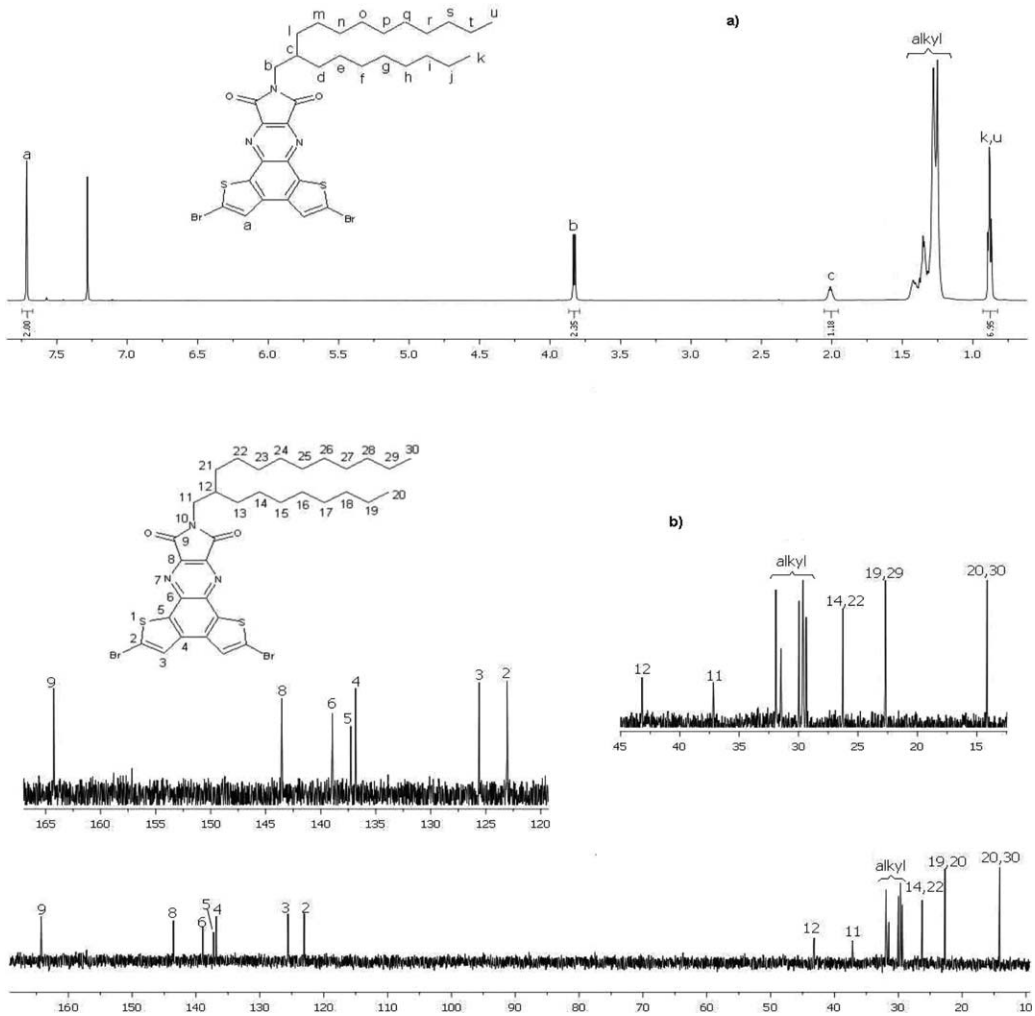

FIGURE 1 (**a**) ^{1}H NMR and (**b**) ^{13}C NMR spectrum of **PTQD**.

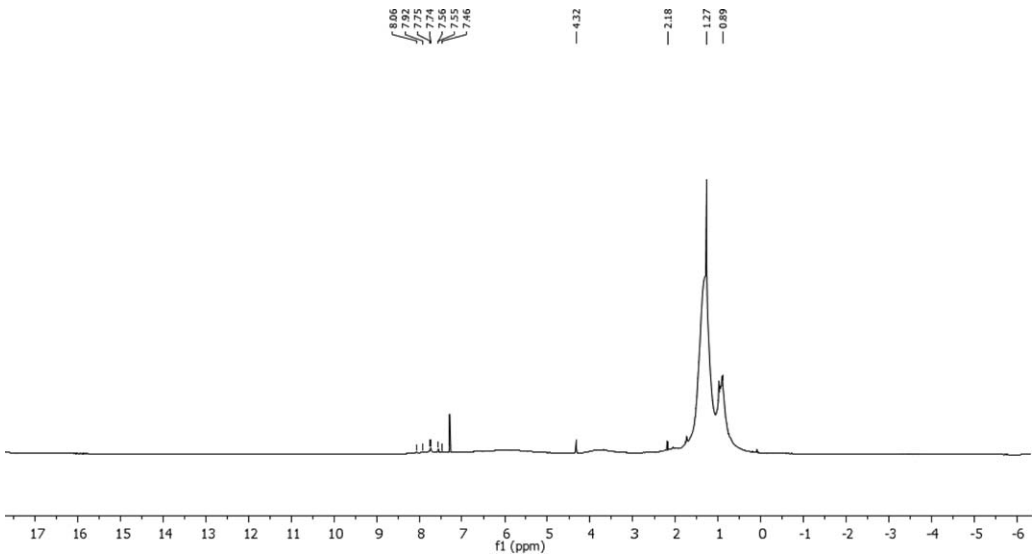

FIGURE 2 ^{1}H NMR of copolymer **P1** in $CDCl_3$.

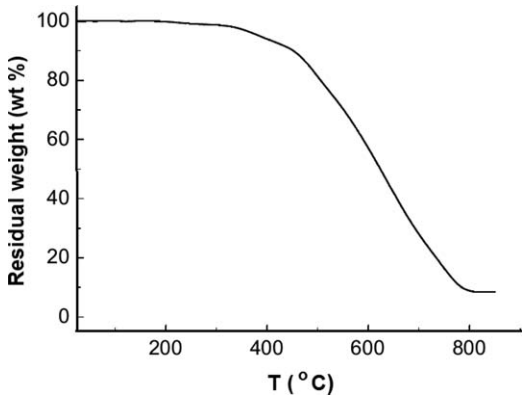

FIGURE 3 TGA curve of copolymer **P1** at the heating rate of 10 °C/min under nitrogen atmosphere.

yield of 71% and relatively high molecular mass, which are well soluble in common organic solvents such as chloroform and chlorobenzene. The average molecular weight (M_n) of **P1** was measured at 13.500 kg/mol with a polydispersity index (PDI) of 2.90. The thermal properties of the copolymer were measured by TGA in a nitrogen atmosphere at a heating rate of 10 °C/min (as shown in Fig. 3). The copolymer exhibited a high thermal stability with onset decomposition temperature with 5% weight-loss (T_d) located at 385 °C.

Optical and Electrochemical Properties

The normalized absorption spectra of copolymer **P1** in dilute chlorobenzene solution and thin film are shown in Figure 4. The copolymer shows the strong absorption ability in solution and as well as the thin film with a wavelength range from 300 to 800 nm and exhibits two absorption bands both in solution and thin film. The absorption spectrum of **P1** in solution showed two main absorption peaks, which are at 378 and 524 nm, respectively and a shoulder around 660 nm. The shorter wavelength band from 340 to 430 nm is assigned to delocalized excitonic π–π^*-transition, while the longer wavelength band with a weak vibronic shoulder in

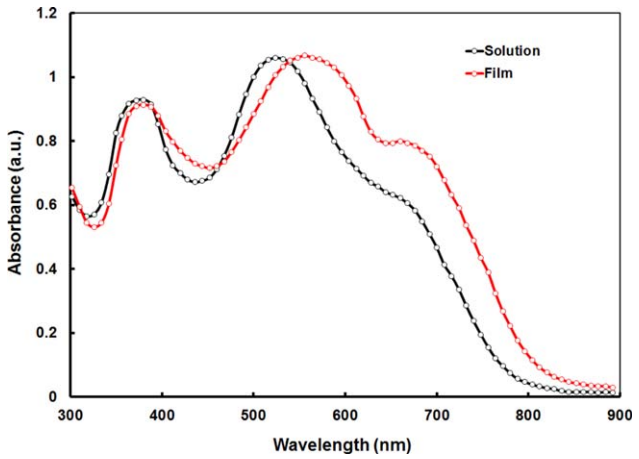

FIGURE 4 UV–visible absorption spectra of **P1** copolymer in chlorobenzene solution and thin film. [Color figure can be viewed in the online issue, which is available at wileyonlinelibrary.com.]

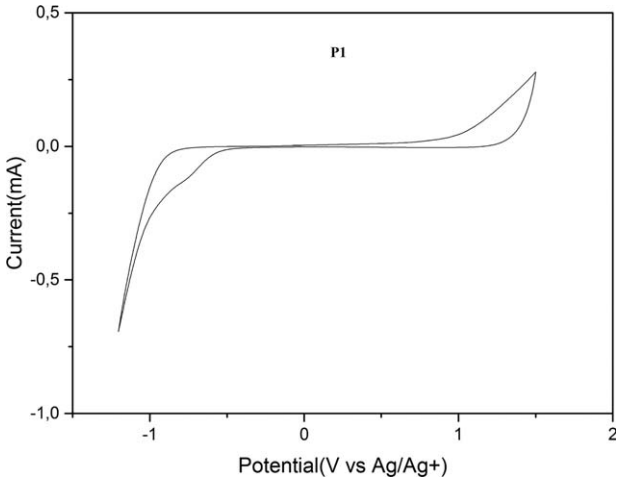

FIGURE 5 Cyclic voltammogram of copolymer **P1** film on platinum electrode in 0.1 mol/L Bu_4NClO_4 in CH_3CN solution at scan rate of 50 mV/s.

the range of 450–800 nm is reasonably ascribed to intramolecular charge transfer (ICT) interactions of donor (thiophene) and acceptor unit (BT and PTQD) of the copolymer backbone. Similar to the absorption in solution, the **P1** film cast from chlorobenzene shows two absorption peaks at 384 and 556 nm, respectively. The absorption band in longer wavelength region has red-shifted and gets broadened as compared with solution, suggesting the presence of intermolecular interactions and aggregation of polymer chain, in solid state. The optical bandgap was estimated from the absorption edge in thin film, which is around 1.50 eV.

The CV was employed to measure the HOMO and LUMO energy levels of the copolymer (Fig. 5). The onset oxidation potential of **P1** was located at 0.96 V, leading to corresponding HOMO level of −5.44 eV. Also from the onset reduction potential (−0.64 V), the LUMO level of **P1** was determined to be −3.84 eV. Thus, the electrochemical bandgap was calculated to be about 1.6 eV. The energy level diagram of the copolymer **P1** and $PC_{71}BM$ are shown in Figure 6. The LUMO gap of 0.36 eV between the copolymer and $PC_{71}BM$ guarantee a sufficient driving force for efficient exciton dissociation at the D–A interface, ensuring energetically favorable electron transfer.[19]

We have additionally performed a theoretical study on the copolymer **P1** molecular structure within the framework of density functional theory (DFT) and time-dependent density functional theory (TD-DFT). The detail is given in Supporting Information.

The geometry optimizations were performed using initial geometries with various orientations of the moieties that compile the copolymer **P1** structure. The main body of the structures is highly planar, with the alkyls oriented off-plane. We have calculated the HOMO and LUMO energy levels and the optical gaps, defined here as the energetically lowest allowed vertical electronic excitation, employing both the

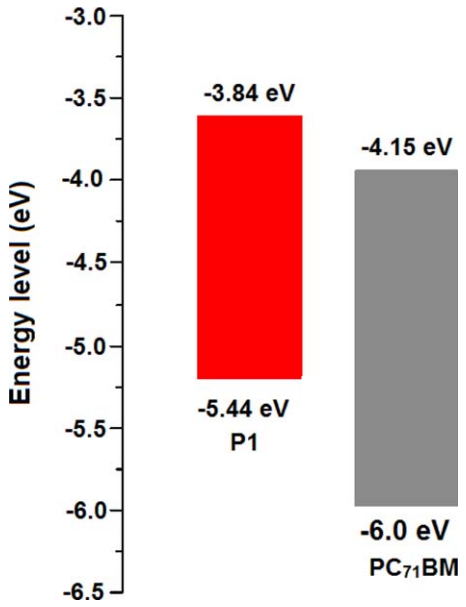

FIGURE 6 HOMO and LUMO energy levels of **P1** and $PC_{71}BM$. [Color figure can be viewed in the online issue, which is available at wileyonlinelibrary.com.]

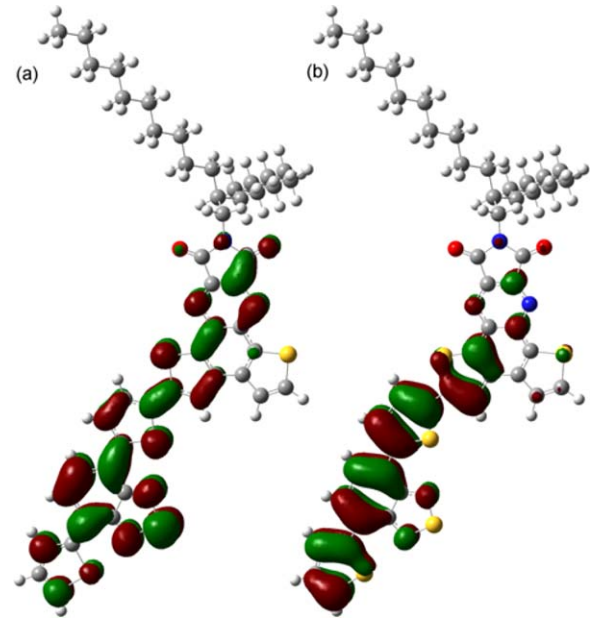

FIGURE 7 (**a**) LUMO and (**b**) HOMO orbitals of **P1** (calculated using the B3LYP functional). [Color figure can be viewed in the online issue, which is available at wileyonlinelibrary.com.]

M06 and B3LYP functionals (see the Table S1, Supporting Information). The HOMO, LUMO, HOMO–LUMO (HL) gap, and optical band gap estimated from B3LYP, when CB solvent effect was taken into account are −5.48, −3.08, 2.39, and 2.04 eV, respectively. In Table S1, Supporting Information, in addition to the frontier orbitals' energy levels, we also provide the optical gap the main contributions to the first excitation as well as the wavelength of the first excitation and of the excitations with the largest oscillator strengths. In addition to the B3LYP functional we have also performed our calculations employing the M06 functional. The M06 meta-hybrid functional was chosen since it provides leveled performance over transition types.

The HL gap calculated using the hybrid B3LYP functional is in good agreement with the experimentally obtained values. The M06 functional produces slightly higher values both for the HL gap and the optical gap. In Table S1, we also provide the character of the first allowed excitations only for contributions larger than 4%. The first excitation, as calculated by both of the functionals, clearly exhibits a single-configuration character. In Figure 7, we have plotted the isosurfaces (isovalue = 0.02) of the HOMO and LUMO, as well as the next nearest frontier orbitals of **P1** which are essentially the only transitions that contribute to the first excitation. Both the HOMO and LUMO extend over a significant portion of the main body of the structure that is planar. We partition the structure into dithiophenebenzothiadiazole (**DTPBTA**) chain moiety and the pyrrolodithienoquinoxalinedione (**PDTQD**) moiety. The delocalization of the HOMO and LUMO over these two regions slightly differs, which results in an intermolecular charge transfer (ICT) from **DTPBTA** to **PDTQD** for the first excitation (taking into account the HOMO to LUMO character of the first excitation). In the Supporting Information (Fig. S2) we also show the isosurfaces of HOMO−1 to HOMO−3, and LUMO+1 to LUMO+3 since transitions between them contribute to the higher energy excitations.

TABLE 1 Photovoltaic Parameters of the BHJ PSCs Based on Active Layers of **P1**:$PC_{71}BM$ in 1:2 Weight Ratio Processed with CB and DIO/CB Solvents

Solvent	J_{sc} (mA/cm^2)	V_{oc} (V)	FF	PCE (%)
CB	9.26	0.88	0.54	4.40 (4.34)[a]
DIO (3 %v)/CB	11.74	0.84	0.63	6.21 (6.13)[a]

[a] Average obtained from of five devices.

The UV/Visual absorption spectra of the **P1** structure calculated at the TD-DFT/B3LYP level of theory, both accounting for solvent effects for CB and in gas phase is shown in Figure S1 (Supporting Information). The spectra have been produced by convoluting Gaussian functions with HWHM = 0.18 eV centered at the excitation wavenumbers. In Figure S3 (Supporting Information), we also provide the corresponding spectra calculated using the M06 functional, which is in good agreement with the spectra using the B3LYP functional and also with the experimental spectra. The absorption spectra of the structure exhibit four main bands that are distributed in a manner that covers a large UV/Vis wavelength range. The bands are centered at 608, 498, 380, and 320 nm. Similar to the first excitation, the ones at 498, 376, and 330 nm also result in ICT from **DTPBTA** to **PDTQD**. Details for the main excitations are given in the Supporting Information. The electronic excitations of **P1** (with non-negligible oscillator strengths, *f*), and the corresponding

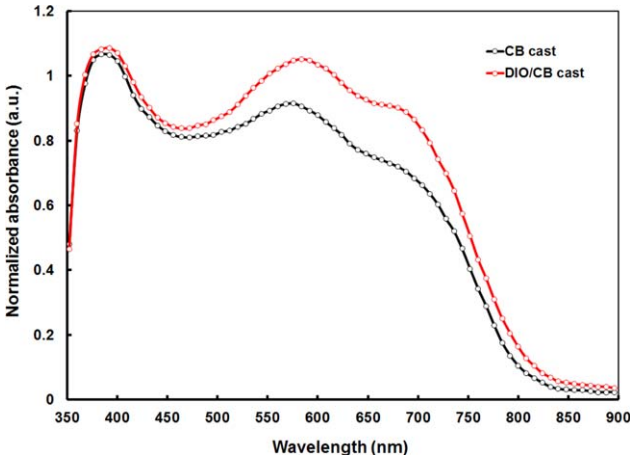

FIGURE 8 Normalized absorption spectra of **P1**:$PC_{71}BM$ (1:2) thin film processed with CB and DIO/CB solvents. [Color figure can be viewed in the online issue, which is available at wileyonlinelibrary.com.]

major contributions, calculated using the B3LYP functional (and CB for solvent) are complied in Table S2 (Supporting Information).

Photovoltaic Properties

In a BHJ PSC, the relative amount of the donor and acceptor materials employed in a blend active layer is a crucial factor for overall PCE, since there should be a balance between absorbance (the photons are mainly absorbed by donor material) and charge carrier (holes and electrons in donor and acceptor phases, respectively) transport in the active layer. When the acceptor content is too low, the electron transporting ability will be limited, while when the acceptor content is high, the absorbance and hole transport ability in the active layer will be decreased. The BHJ active layers with the mixture of **P1** and $PC_{71}BM$ blended in CB in different weight ratios (1:1, 1:1.5, 1:2, and 1:2.5) were prepared and their photovoltaic performances were investigated and listed in Table S3, Supporting Information. The donors to acceptor weight ratio significantly affect the overall PCE of the device and mainly attributed to the J_{sc} and FF. The optimum device performance was found for the 1:2 ratio. It is found that when the ratio is 1:2.5, the PCE decreases to 3.76% owing to the decrease in J_{sc} and FF to 8.58 mA/cm^2 and 0.51, respectively, because of the decrease in the light harvesting ability of the active layer and poor hole transport. Therefore, we are only describing the results for the optimized active layer with donor to acceptor ratio of 1:2.

The normalized absorption spectrum of **P1**:$PC_{71}BM$ (1:2) processed from CB solvent is shown in Figure 8 (black color). It can be seen from the Figure 8 that the spectrum shows the combination of both **P1** and $PC_{71}BM$ absorptions, indicating the both **P1** and $PC_{71}BM$ contribute in light absorption and photocurrent generation.

The current–voltage (*J*–*V*) characteristics under AM1.5 (100 mW/cm^2) simulated solar illumination of BHJ organic solar cell with optimized **P1**:$PC_{71}BM$ (1:2 w/w) blend processed from CB solvent are shown in Figure 9(a) (black color) and photovoltaic parameters are summarized in Table 1. The device showed an overall PCE of 4.24%, with J_{sc} = 9.26 mA/cm^2, V_{oc} = 0.88 V, and FF = 0.52. The respectable value of V_{oc} may be due to the deep HOMO energy level of **P1**, since the V_{oc} of the BHJ organic solar cells is directly related to the energy difference between the HOMO energy level of donor and the LUMO energy level of the acceptor.

The IPCE spectrum of the CB solvent processed BHJ organic solar cell based on the **P1**:$PC_{71}BM$ with weight ratio 1:2 (w/w) is shown in Figure 9(b) (black color) and the IPCE spectrum closely resembles with the optical absorption spectrum of **P1**:$PC_{71}BM$ (1:2 w/w) blended thin film (Fig. 8), indicating both **P1** and $PC_{71}BM$ contribute to the exciton generation after the absorption of photons by the active layer. The PCE of copolymer **P1** having D–A_1–D–A_2 structure based device is higher than that for D–A_2 copolymer (PCE = 3.65%)[20] as reported by us.

The overall PCE of the BHJ PSC with **P1**:$PC_{71}BM$ active layer processed with CB solvent is poor, as compared with the

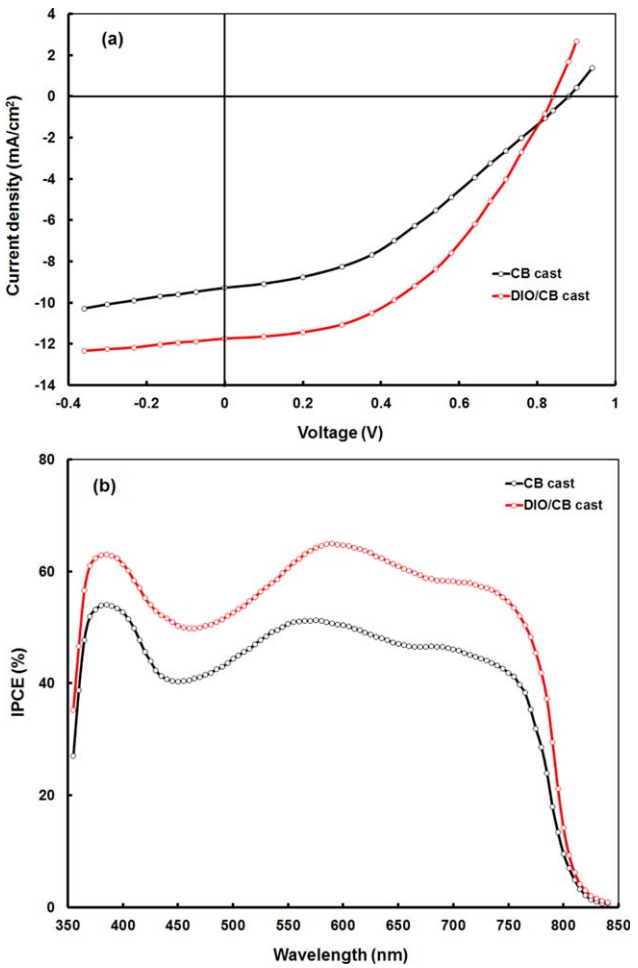

FIGURE 9 (**a**) Current–voltage (*J*–*V*) characteristics and (**b**) IPCE spectra of **P1**:$PC_{71}BM$ (1:2 w/w) devices processed with CB and DIO/CB solvents. [Color figure can be viewed in the online issue, which is available at wileyonlinelibrary.com.]

latest developments on other low bandgap polymer based solar cells. Since the V_{oc} (0.88 V) of present solar cell is quite respectable, its poor performance can be attributed to the low J_{sc} and FF. These two parameters are directly related to light harvesting ability of the active layer, film morphology, exciton dissociation, and transfer at D/A interfaces present in the BHJ active layer, and charge transport through the active layer, toward the electrodes (holes and electrons toward the anode and cathode, respectively). A well defined nanomorphology and phase separation between donor and acceptor components in the active layer within the range of exciton diffusion length is necessary for efficient exciton dissociation and charge transport.[1a]

Apart from the intrinsic properties of the active layer, the morphology of blend including the crystallinity of polymers,[21] domain size,[22] miscibility of donor and acceptor materials,[23] and molecular orientation[24] are also important for over PCEs of BHJ PSCs. Various strategies such as solvent annealing,[25] thermal annealing,[26] and selection of solvent,[27] or mixed solvent,[28] have been employed to control the morphology of BHJ active layers. Among them, the addition of solvent processing additive is one of the simplest but most effective methods, since the addition of a small amount of solvent processing additives can affect the size of fullerene domains by improving its solubility in most of the common organic solvents over that of the polymers.[29] The solvent mixtures containing a poor solvent for conjugated polymers have been employed to control the morphology of blend active layer. Moreover, the elongated drying time for film formation, due to the high boiling point of solvent additive allows the donor polymer to be self organized, which tunes the thin film morphology of BHJ layer to be favorable for exciton dissociation, resulting enhanced PCEs of PSCs. The advantage of processing additive approach is that phase separated morphology develops in the active layer through the use of single step spin coating process without any post treatment. Moreover, the crystallinity of polymer and domain sizes of donor and acceptor in the blend can be tuned effectively by using solvent additive approach and play an important role in enhancing the overall performance of the organic solar cells.

We have used most popular approach i.e. solvent additive, to improve the performance of BHJ PSC using **P1**:$PC_{71}BM$ (1:2 w/w) active layer and varied the concentration of 1,8-diiodooctane (DIO), 1%, 2%, 3%, and 4% (v/v, DIO/CB) and found that the optimized concentration was 3 vol %. The concentration dependence of solvent additive (DIO) on the photovoltaic performance of device based on **P1**:$PC_{71}BM$ is displayed in Table S4 (Supporting Information). After increasing the concentration solvent additive (DIO) beyond 3% vol, the device performance was declined, attributed to the fact the some of the solvent residue remains in the film and not properly dried. Since the photovoltaic performance of organic solar cell also depends on the thickness of the active layer mainly attributed to the charge carrier mobility. We have taken much care to ensure alike film thickness of the active layer (90 ± 5 nm) and avoid substantial influence of this parameter on the devices charge mobility. Figure 9(a,b - red color) shows the *J–V* characteristics and IPCE spectrum of solar cells, respectively, based on **P1**:$PC_{71}BM$ (1:2 w/w) blend spin coated with DIO (3 vol %)/CB solvent and photovoltaic parameters were summarized in Table 1. The optimal PCE of 5.92% was obtained with $J_{sc} = 11.74$ mA/cm^2, $V_{oc} = 0.84$ V, and FF = 0.60. The enhancement in the PCE of later device is attributed to its improved J_{sc} and FF values. The higher value of J_{sc} is ascribed to the improved value of IPCE covering wide range [Fig. 9(b)]. The J_{sc} values obtained by integrating the IPCE spectrum are about 9.04 and 11.52 mA/cm^2 for the device processed without and with DIO additive, which are slightly smaller than the measured values (from *J–V* characteristics under illumination). In contrary, there is a small reduction in V_{oc} from 0.88 to 0.84 V, suggesting that ordering of the active layer is induced by DIO, which is usually favorable for charge transport.[30]

The values of IPCE and J_{sc} of the organic BHJ solar cells are closely related to the light harvesting efficiency of the active layer employed. As shown in Figure 8, the absorption maximum of the **P1**:$PC_{71}BM$ film is about 568 nm, when 3 vol % of DIO added to the host CB solvent, the absorption intensity in the region 450–800, increases, which is indicative of the close packing of **P1** and redshift of absorption band. Moreover, the intensity of shoulder at 680 nm is also slightly increased.

The incorporation of DIO additive into **P1**:$PC_{71}BM$ blend results in a close packing of **P1** and better phase separation of **P1** and $PC_{71}BM$. The addition of processing additives to **P1**:$PC_{71}BM$ blend film increases the strengths of intermolecular interactions between the **P1** and $PC_{71}BM$, and processing additives.[31] The increase in the absorption intensity of **P1**:$PC_{71}BM$ film, particularly the wavelength region corresponds to copolymer leads to the enhancement in the light harvesting efficiency of the device and more excitons are generated, resulting higher photocurrent.

We have also estimated the series (R_s) and shunt (R_{sh}) resistance of the devices, from the slope of the *J–V* characteristics of devices under illumination around open circuit voltage and slope in the third quardant of *J–V* characteristics [Fig. 9(a)] and complied in Table 2. The device based on the active layer **P1**:$PC_{71}BM$ (1:2) processed with DIO additive showed larger R_{sh} as compared with the device without additive. It is well known that the leakage current is determined by the shunt resistance (R_{sh}).[32] The larger R_{sh} indicates a lower charge carrier recombination in the active layer. This indicates DIO additive can effectively restrain the leakage current under the reverse bias, which may provide effective charge carrier transport in the blend layer, resulting in the increase in J_{sc}, compared with the device without additive. The smaller R_s indicates a lower resistance of the active layer and better metal/active layer interface connection induced by using additive.[26a]

The well nanoscale morphology of the BHJ active layer is important for the efficient organic solar cell. To get information

TABLE 2 Series Resistance (R_s), Shunt Resistance (R_{sh}), Charge Carrier Mobilities of the Devices Based in **P1**:$PC_{71}BM$ in 1:2 Weight Ratio Processed with CB and DIO/CB Solvents

Solvent	R_s (Ω cm$^{2)}$	R_{sh} (Ω cm^2)	μ_h (cm^2/Vs) $\times 10^{-5}$	μ_e (cm^2/Vs) $\times 10^{-4}$	μ_e/μ_h
CB	12	378	1.56	2.46	15.7
DIO (3 %v)/CB	5.6	673	8.78	2.38	2.71

about the morphology and phase separation, we have recorded the transmission electron microscopy (TEM) of the **P1**:$PC_{71}BM$ film prepared from CB and (DIO 3 vol %)/CB (Fig. 10). The film cast from CB clearly shows larger dark domains with diameters between 60 and 100 nm. The dark and larger domains in the TEM images were assigned to crystalline **P1** domains in the **P1**:$PC_{71}BM$ blend.[33] After addition of DIO, as a processing additive, the large domains were reduced significantly, suggesting the decrease in **P1** crystallinity was accompanied with the shrinkage of darker crystalline **P1** domains. Thus addition of DIO reduces the crystallinity of **P1** suppresses the phase aggregation in the blend film. As shown in atomic force microscopy (AFM) images (Fig. 11), the surface of the film processed with CB in non-uniform with root mean square (RMS) roughness value of 3.78 nm, because of relatively large domain on the surface, whereas after adding 3 vol % DIO, the film become relatively more uniform with a lower RMS value of 1.52 nm. These results indicate the phase separation of **P1** and $PC_{71}BM$ is enhanced and therefore the more appropriate interpenetrating network may be formed with the addition of DIO. This might enhance the transport and collection of charge carrier,[34] which resulted in the improvement of J_{sc} and FF.

In order to get information about the solvent additive on the crystallinity of the optimized film **P1**:$PC_{71}BM$ blended film, we have recorded the X-ray pattern of the film cast from CB and DIO (3 vol %)/CB and shown in Figure 12. It can be seen that the XRD pattern of both the film cast either CB or DIO/CB solvent showed a peak around $2\theta = 7.6^\circ$ which is corresponds to the d-spacing of the copolymer **P1**. The intensity of peak correspond to **P1** increased significantly upon the addition of DIO into the host CB solvent, indicated that the strong improvement of the crystallinity of the copolymer, due to the high boiling point of DIO, the active layer film dried slowly, which assisted the formation of a self-ordered structure in the blend. Additionally, more intense diffraction peak also indicates the higher crystallinity of the film, leading to an increase in the hole mobility and leads to an increase in J_{sc} of the corresponding device.

We have examined the effect of the additive on the photocurrent density (J_{ph}). The J_{ph} was estimated as $J_{ph} = J_L - J_D$, where J_L and J_D are the current densities under illumination and in the dark, respectively. Figure 13 shows the variation of J_{ph} with the effective voltage ($V_{eff} = V_0 - V$, where V_0 is the compensation voltage at which J_{ph} is zero and V is applied voltage) for the devices. It can be seen from these plots that the J_{ph} was saturated at high value of V_{eff}. The saturation photocurrent density (J_{phsat}) is only limited by the total amounts of absorbed photons if we assume that all the photogenerated excitons are dissociated into free charge carriers and collected by the electrodes at a high V_{eff}.[35] J_{satph} was 9.98 and 12.95 mA/cm^2 for the devices processed without and without DIO additives, respectively. The increased J_{satph} may be attributed to the effective charge transport and collection for the device with DIO additive.[36] To gain more information about the influence of solvent additive on the exciton generation, we have measured the maximum exciton generation rate (G_{max}) of the devices using $J_{phsat} = qG_{max}\ L$, where L is the thickness of the active layer ($\sim$90 nm). From

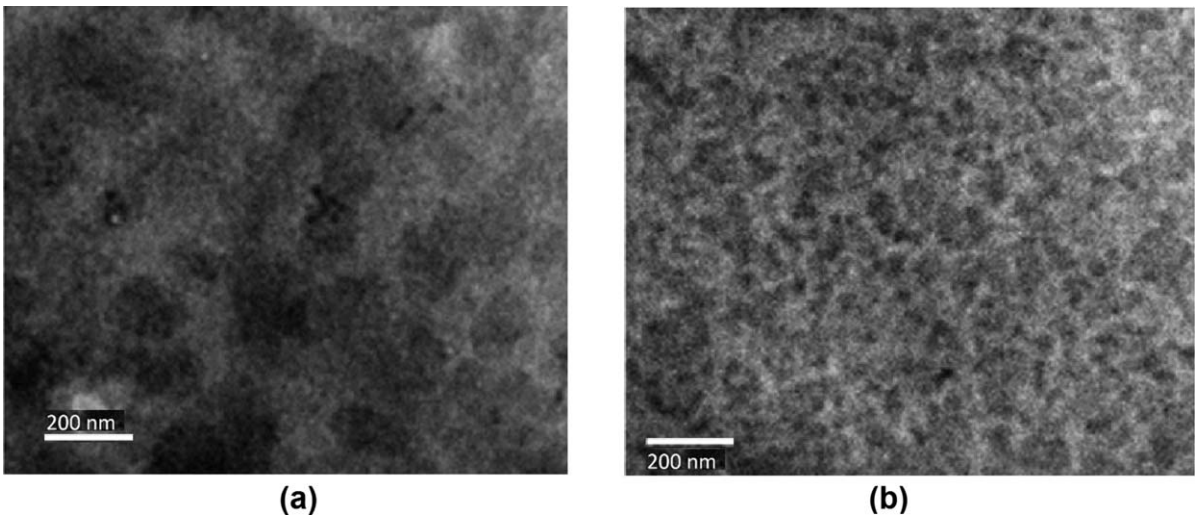

FIGURE 10 TEM images of **P1**:$PC_{71}BM$ (1:2 w/w) films processed with (**a**) CB and (**b**) DIO/CB solvents.

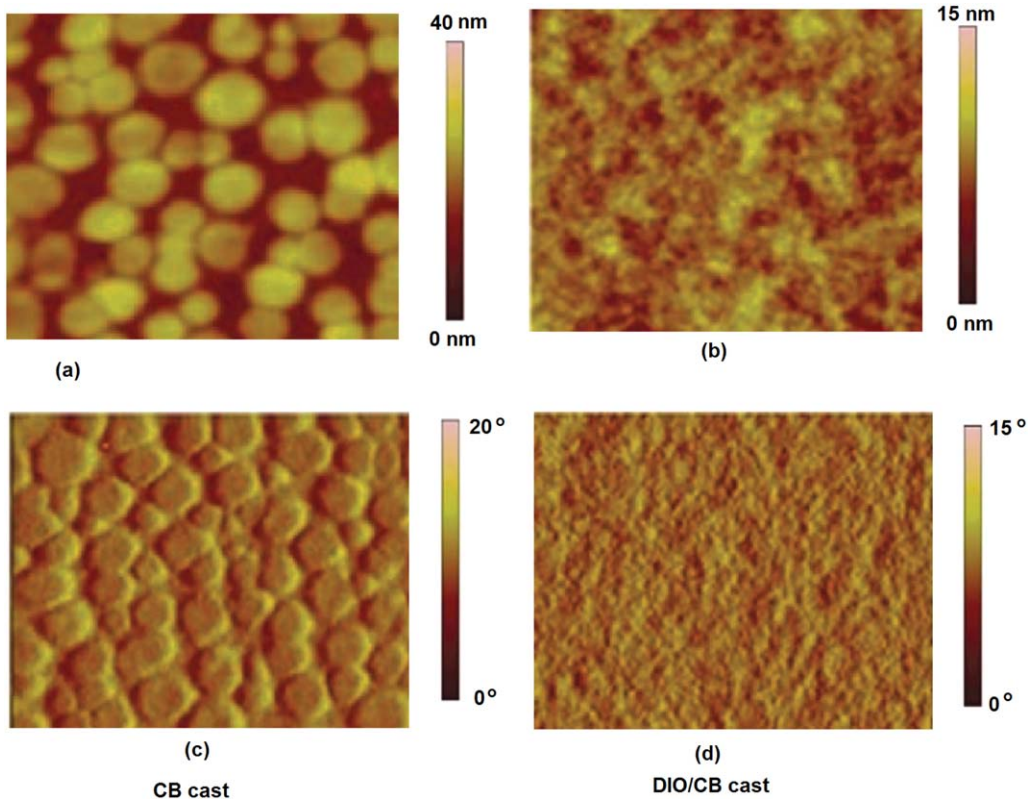

FIGURE 11 AFM height images (**a** and **b**) and phase images (**c** and **d**) of **P1**:$PC_{71}BM$ (1:2 w/w) films processed with CB and DIO/CB solvents, image size is 3 μm × 3 μm. [Color figure can be viewed in the online issue, which is available at wileyonlinelibrary.com.]

Figure 13, the values of G_{max} were found around 6.93 × $10^{27}/m^3s$ and 9.0 × $10^{27}/m^3s$, for the devices without and with DIO solvent additives, respectively. G_{max} increased after the addition of DIO, suggesting light absorption by the active layer used in the device was increased. This is consistent with the increased absorption of active layer as shown in the Figure 8.

To find the origin of difference in the performances of the solar cells processed with and without DIO, the charge transport properties were investigated by examining the charge carrier mobility of **P1**:$PC_{71}BM$, under each optimized conditions by using space charge limited current model for hole only (ITO/PEDOT:PSS/**P1**:$PC_{71}BM$/Au) device and electron only device (ITO/Al/**P1**:$PC_{71}BM$/Al device).[35] Hole and electron mobilities were calculated by the Mott–Gurney Law, in which the current density (J_{SCLC}) in SCLC expressed as

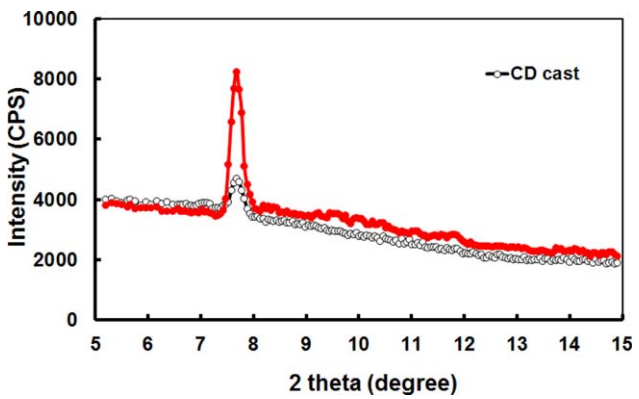

FIGURE 12 XRD patterns of **P1**:$PC_{71}BM$ cast from CB and DIO/CB solvents. [Color figure can be viewed in the online issue, which is available at wileyonlinelibrary.com.]

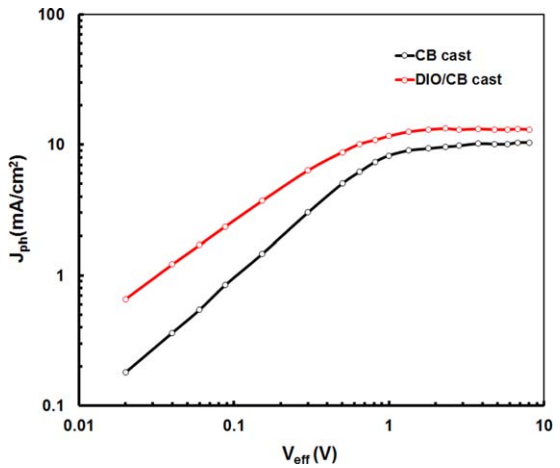

FIGURE 13 Photocurrent density versus effective voltage (J_{ph}–V_{eff}) characteristics of devices without and 3 v/v% DIO solvent additive processed active layers. [Color figure can be viewed in the online issue, which is available at wileyonlinelibrary.com.]

$$J_{SCLC} = \frac{9}{8}\varepsilon_o\varepsilon_r\mu\frac{V^2}{L^3}$$

where ε_o, ε_r are the permittivity of free space and relative dielectric constant of active layer, respectively, μ is the charge carrier mobility, V is the internal voltage, that is, $V = V_{app} - V_{bi}$ (V_{bi} is the built in potential arise due to the work function difference between the anode and cathode), and L is the thickness of the active layer. The J–V characteristics of the hole-only devices based on **P1**:$PC_{71}BM$ thin films processed with and without DIO are shown in Figure 14. The hole mobility values for CB and DIO/CB processed **P1**:$PC_{71}BM$ thin films were found to be 1.56×10^{-5} and 8.78×10^{-5} cm^2/Vs, respectively. The increased value of hole mobility for latter film compared with former one may be attributed to the suppression of phase aggregation and increase in percolative pathways for hole transport.[36] On contrary, the electron mobility was found to be slightly decreased for the DIO/CB processed film, that is, 2.46×10^{-4} and 2.38×10^{-4} cm^2/Vs for CB and DIO/CB cast film, respectively, obtained in similar manner. In a BHJ organic solar cell, both transport of electrons and holes contribute to the photocurrent generation and these are to be balanced to achieve the high J_{sc} and FF, that is, the electron/hole mobility ratio should be as low as possible (unity for ideal solar cell). For CB and DIO/CB processed devices, this ratio is 15.76 and 2.71, respectively. The improved balance of charge transport between the electron and hole in the active layer spun cast with DIO/CB solvent leads to efficient charge transport and collection and might be another reason for the enhanced J_{sc}, FF, and PCE values of the device.

We have also measured the J_{sc} at different illumination intensities to get information about the charge recombination kinetics. The variation of J_{sc} with illumination intensity is shown in Figure 15, in which data are plotted in log–log scale and fitted to power law (solid lines). In most of the organic solar cells, a power law dependence of J_{sc} on illumination intensity (P_{in}) is observed, that is, $J_{sc} \propto P_{in}^{\alpha}$. The exponential factor $\alpha = 1$ is indicative of efficient swept out of charge carriers before the occurrence of recombination.[37] The estimated value of α for the device processed without and with DIO additive are 0.91 and 0.94, respectively. The increased value of α for the device processed with DIO additives implies that the swept out of charge carrier is more effective in this device. This is in agreement with the more balanced charge transport observed from the mobility measurements. The lower value of α for the device processed with CB only suggests that the bimolecular recombination is more important in this device. An unbalanced hole and electron mobility in this device can also be attributed to the lower value of α.

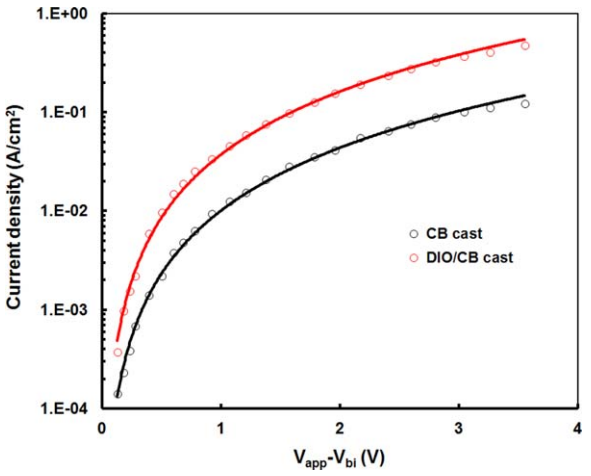

FIGURE 14 Current–voltage ($J-V$) characteristics in dark for hole-only devices based on **P1**:$PC_{71}BM$ (1:2 w/w) processed with CB and DIO/CB solvents. [Color figure can be viewed in the online issue, which is available at wileyonlinelibrary.com.]

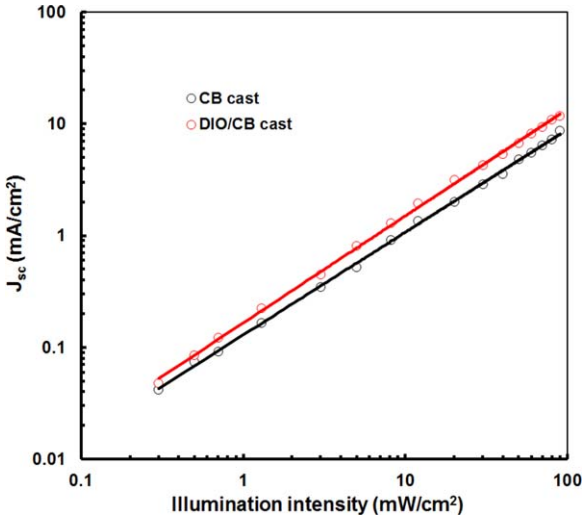

FIGURE 15 Variation of J_{sc} with illumination intensity for devices based on **P1**:$PC_{71}BM$ (1:2 w/w) processed with CB and DIO/CB solvents. [Color figure can be viewed in the online issue, which is available at wileyonlinelibrary.com.]

CONCLUSIONS

A new solution processed D–A_1–D–A_2 copolymer denoted as **P1** with two electron withdrawing units having different acceptor strength, that is, PTQD and BT and thiophene donor was designed and synthesized. The targeted copolymer exhibited high thermal stability, broad absorption spectral profile matched with solar spectrum, and deep HOMO energy level. The device based on optimized **P1**:$PC_{71}BM$ (1:2) spun cast with CB and DIO/CB solvent showed a PCE of 4.40% ($J_{sc} = 9.26$ mA/cm^2, $V_{oc} = 0.88$ V, and FF = 0.54) and 6.21% ($J_{sc} = 11.74$ mA/cm^2, $V_{oc} = 0.84$ V, and FF = 0.63), respectively. The incorporation of 3 vol % DIO in the host CB solvent increases the absorption intensity of **P1**:$PC_{71}BM$ blend, particularly the absorption band corresponds to **P1** and phase separation between **P1** and $PC_{71}BM$, enhances the J_{sc} and FF, resulting an improvement in the overall PCE. These results demonstrate that a copolymer with a combination of strong acceptor and weak acceptor may be a promising electron donor for high performance solution processable BHJ PSCs.

ACKNOWLEDGMENT

M.L. Keshtov, S.A. Kuklin, and D.Y. Godovsky are thankful to Russian Science Foundation (grant number 14-13-01444).

References and Notes

1 (a) Y. Li, *Acc. Chem. Res.* **2012**, *45*, 723–733; (b) B. C. Thompson, P. P. Khlyabich, B. Burkhart, A. E. Aviles, A. Rudenko, G. V. Shultz, C. F. Ng, L. B. Mangubat, *Green* **2011**, *1*, 29–54; (c) G. Li, R. Zhu, Y. Yang, *Nat. Photonics* **2012**, *6*, 153–161; (d) L. Dou, J. You, Z. Hong, Z. Xu, G. Li, R. A. Street, Y. Yang, *Adv. Mater.* **2013**, *25*, 6642–6671; (e) F. C. Krebs, N. Espinosa, M. Hösel, R. R. Søndergaard, M. Jørgensen, *Adv. Mater.* **2014**, *26*, 29–39; (f) I. Etxebarria, J. Ajuria, R. Pacios, *Org. Electron.* **2015**, *19*, 34–60.

2 (a) L. T. Dou, C. C. Chen, K.; Yoshimura, K. Ohya, W. H. Chang, J. Cao, Y. S. Liu, E. Richard, Y. Yang, *Macromolecules* **2013**, *46*, 3384–3390; (b) S. J. Liu, K. Zhang, J. M. Lu, J. Zhang, H. L. Yip, F. Huang, Y. Cao, *J. Am. Chem. Soc.* **2013**, *135*, 15326–15329; (c) M. J. Zhang, Y. Gu, X. Guo, F. Liu, S. Q. Zhang, L. J. Hou, T. P. Russell, J. H. Hou, *Adv. Mater.* **2013**, *25*, 4944–4949; (d) S. H. Liao, H. J. Jhuo, Y. S. Cheng, S. A. Chen, *Adv. Mater.* **2013**, *25*, 4766–4771.

3 (a) Z. C. He, C. M. Zhong, S. J. Su, M. Xu, H. B. Wu, Y. Cao, *Nat. Photonics* **2012**, *6*, 591–595; (b) H. Y. Chen, J. H. Hou, S. Q. Zhang, Y. Y. Liang, G. W. Yang, Y. Yang, L. P. Yu, Y. Wu, G. Li, *Nat. Photonics* **2009**, *3*, 649–653; (c) X. Guo, M. J. Zhang, W. Ma, L. Ye, S. Q. Zhang, S. J. Liu, H. Ade, F. Huang, J. H. Hou, *Adv. Mater.* **2014**, *26*, 4043–4049; (d) T. L. Nguyen, H. Choi, S.-J. Ko, M. A. Uddin, B. Walker, S. Yum, J. E. Jeong, M. H. Yun, T. J. Shin, S. Hwang, J. Y. Kim, H. Y. Woo, *Energy Environ. Sci.* **2014**, *7*, 3040–3051; (e) L. Ye, S. Q. Zhang, W. C. Zhao, H. F. Yao, J. H. Hou, *Chem. Mater.* **2014**, *26*, 3603–3605; (f) L. Lu, L. Yu, *Adv. Mater.* **2014**, *26*, 4413–4430; (g) C. C. Chen, W. H. Chang, K. Yoshimura, K. Ohya, J. B. You, J. Gao, Z. Hong, Y. Yang, *Adv. Mater.* **2014**, *26*, 5670–5677; (h) L. Ye, S. Q. Zhang, W. C. Zhao, H. F. Yao, J. H. Hou, *Chem. Mater.* **2014**, *26*, 3603–3605.

4 (a) J. B. You, L. T.; Dou, K. Yoshimura, T. Kato, K. Ohya, T. Moriarty, K. Emery, C. C. Chen, J. Gao, G. Li, Y. Yang, *Nat. Commun.* **2013**, *4*, 1446; (b) A. R. M. Yosoff, D. Kim, H. Kim, F. K. Shneider, W. J. da Silva, J. Jang, *J. Energy Environ. Sci.* **2015**, *8*, 303–316; (c) S. H. Liao, H. J. Jhou, P. N. Yeh, Y. S. Cheng, Y. Li, Y. H. Lee, S. Sharma, S. A. Chen, *Sci. Rep.* **2014**, *4*, 6813; (d) Y. Lin, J. Zhao, Z. Li, C. Mu, W. Ma, H. Hu, K. Jiang, H. Lin, H. Ade, H. Yan, *Nat. Commun.* **2014**, *5*, 5293; (e) C. Liu, C. Yi, K. Wang, Y. Yang, R. Bhatt, M. Tsige, S. Xiao, X. Gong, *ACS Appl. Mater. Interfaces* **2015**, *7*, 4928–4935.

5 (a) C. Gao, L. Wang, X. Li, H. Wang, *Polym. Chem.* **2014**, *5*, 5200–5210; (b) R. Stalder, J. Mei, K. R. Graham, L. A. Estrada, J. R. Reynolds, *Chem. Mater.* **2014**, *26*, 664–678; (c) H. J. Son, B. Carsten, I. H. Jung, L. Yu, *Energy Environ. Sci.* **2012**, *5*, 8158–8170.

6 M. C. Scharber, N. S. Sariciftci, *Prog. Polym. Sci.* **2013**, *38*, 1929–1940.

7 N. Li, D. Baran, G. D. Spyropoulos, H. Zhang, S. Berny, M. Turbiez, T. Ameri, F. C. Krebs, C. J. Brabec, *Adv. Energy Mater.* **2014**, *4*, 1400084.

8 Y. F. Li, Y. P. Zou, *Adv. Mater.* **2008**, *20*, 2952–2958.

9 J. W. Chen, Y. Cao, *Acc. Chem. Res.* **2009**, *42*, 1709–1718.

10 (a) S. C. Rasmussen, S. J. Evenson, *Prog. Polym. Sci.* **2013**, *38*, 1773–1804; (b) A. Pron, M. Leclerc, *Prog. Polym. Sci.* **2013**, *38*, 1815–1831; (c) J. S. Wu, W. Cheng, Y. J. Cheng, C. S. Hsu, *Chem. Soc. Rev.* **2015**, *44*, 1113–1154.

11 (a) Y. Lin, Y. Li, X. Zhan, *Chem. Soc. Rev.* **2012**, *41*, 4245–4272; (b) Y. Chen, X. Wan, G. Long, *Acc. Chem. Res.* **2013**, *46*, 2645–2655; (c) Y. Li, *Acc. Chem. Res.* **2012**, *45*, 723–733.

12 (a) K. H. Hendriks, G. H. L. Heintges, V. S. Gevaerts, M. M. Wienk, R. A. J. Janssen, *Angew. Chem., Int. Ed.* **2013**, *52*, 8341–8344; (b) C. Kanimozhi, N. Yaacobi-Gross, K. W. Chou, A. Amassian, T. D. Anthopoulos, S. Patil, *J. Am. Chem. Soc.* **2012**, *134*, 16532–16535; (c) T. Qin, W. Zajaczkowski, W. Pisula, M. Baumgarten, M. Chen, M. Gao, G. Wilson, C. D. Easton, K. Müllen, S. E. Watkins, *J. Am. Chem. Soc.* **2014**, *136*, 6049–6055; (d) M. Wang, H. Wang, T. Yokoyama, X. Liu, Y. Huang, Y. Zhang, T. Q. Nguyen, S. Aramaki, G. C. Bazan, *J. Am. Chem. Soc.* **2014**, *136*, 12576–12579; (e) T. E. Kang, K. H. Kim, B. J. Kim, *J. Mater. Chem. A* **2014**, *2*, 15252–15267; (f) X. Huang, G. Zhang, C. Zhou, L. Liu, Y. Jin, S. Liu, L. Ying, F. Huang, Y. Cao, *Polym. Chem.* **2015**, *6*, 4154–4161.

13 (a) J. D. Yuen, J. Fan, J. Seifter, B. Lim, R. Hufschmind, A. J. Heeger, F. Wudl, *J. Am. Chem. Soc.* **2011**, *133*, 20799–20807; (b) Q. Shi, H. Fan, Y. Liu, W. Hu, Y. Li, X. Zhan, *J. Phys. Chem. C* **2010**, *114*, 16843–16848; (c) S. Subramaniyan, F. S. Kim, G. Ren, H. Li, S. A. Jenekhe, *Macromolecules* **2012**, *45*, 9029–9037.

14 (a) D. Dang, W. Chen, R. Yang, W. Zhu, W. Mammod, E. Wang, *Chem. Commun.* **2013**, *49*, 9335–9337; (b) W. Sun, Z. Ma, D. Dang, W. Zhu, M. R. Andersson, F. Zhang, E. Wang, *J. Mater. Chem. A* **2013**, *1*, 11141–11144.

15 Q. Tao, Y. Xia, X. Xu, S. Hedstrom, O. Backe, D. I. James, P. Persson, E. Olsson, O. Inganäs, L. Hou, W. Zhu, E. Wang, *Macromolecules* **2015**, *48*, 1009–1016.

16 (a) R. Qin, W. Li, C. Li, C. Du, C. Veit, H.-F. Schleiermacher, M. Andersson, Z. Bo, Z. Liu, O. Inganäs, U. Wuerfel, F. Zhang, *J. Am. Chem. Soc.* **2009**, *131*, 14612–14613; (b) E. Zhou, J. Cong, K. Hashimoto, K. Tajima, *Macromolecules*, **2013**, *46*, 763–768.

17 D. J. Cram, H. J. Choi, J. A. Byrant, B. K. Carolyn, *J. Am. Chem. Soc.* **1992**, *114*, 7748–7765.

18 J. A. Letizia, M. R. Salata, C. M. Tribout, A. Facchetti, M. A. Ratner, T. J. Marks, *J. Am. Chem. Soc.* **2008**, *130*, 9679–9694.

19 C. J. Brabec, C. Winder, N. S. Sariciftci, J. C. Hummelen, A. Dhanabalan, P. A. van Hal, R. A. J. Janssen, *Adv. Funct. Mater.* **2002**, *12*, 709–712.

20 M. L. Keshtov, S. A. Kuklin, F. C. Chen, A. R. Khokhlov, A. S. Peregudov, S. A. Siddiqui, G. D. Sharma, *Org. Electron.* **2015**, *24*, 135–146.

21 (a) D. Credgington, R. Hamilton, P. Atienzar, J. Nelson, J. R. Durrant, *Adv. Funct. Mater.* **2011**, *21*, 2744–2753; (b) P. E. Keivanidis, V. Kamm, W. Zhang, G. Fluoudas, F. Laquai, I. McCulloch, D. D. C. Bradley, J. R. Nelson, *Adv. Funct. Mater.* **2012**, *22*, 2318–2326; (c) H. Mangold, A. A. Bakulin, I. A. Howard, C. Kastner, D. A. M. Egbe, H. Hoppe, F. Liquai, *Phys. Chem. Chem. Phys.* **2014**, *16*, 20329–20337.

22 (a) C. J. Schaffer, C. M. Palumbiny, M. A. Niedermeier, C. Jendrzejewski, G. Santoro, S. V. Roth, P. Müller-Buschbaum, *Adv. Mater.* **2013**, *25*, 6760–6764; (b) O. V. Mikhnenko, H. Azimi, M. Scharber, M. Morana, P. W. M. Blom, M. A. Loi, *Energy Environ. Sci.* **2012**, *5*, 6960–6965; (c) W. A. Luhman, R. J. Holmes, *Adv. Funct. Mater.* **2011**, *21*, 764–771.

23 E. Zhou, J. Cong, K. Hashimoto, K. Tajima, *Adv. Mater.* **2013**, *25*, 6991–6996.

24 J. R. Tumbleston, B. A. Collins, L. Yang, A. C. Stuart, E. Gann, W. Ma, W. You, H. Ade, *Nat. Photonics* **2014**, *8*, 385–391.

25 (a) G. Li, V. Shrotriya, J. Huang, Y. Yao, T. Moriarty, K. Emery, Y. Yang, *Nat. Mater.* **2005**, *4*, 864–868; (b) J. H. Park, J. S. Kim, J. H. Lee, W. H. Lee, K. Cho, *J. Phys. Chem. C* **2009**, *113*, 17579–17584.

26 (a) F. Padinger, R. S. Rittberger, N. S. Sariciftci, *Adv. Funct. Mater.* **2003**, *13*, 85–88; (b) C. R. McNeill, J. J. M. Halls, R. Wilson, G. L. Whiting, S. Berkebile, M. G. Ramsey, R. H. Friend N. C. Greenham, *Adv. Funct. Mater.* **2008**, *18*, 2309–2321.

27 (a) S. H. Park, A. Roy, S. Beaupre, S. Cho, N. Coates, J. S. Moon, D. Moses, M. Leclerc, K. Lee, A. J. Heeger, *Nat. Photonics* **2009**, *3*, 297–302; (b) C. W. Rochester, S. A. Mauger, A. J. Moulé, *J. Phys. Chem. C* **2012**, *116*, 7287–7292; (c) Y. Liang, Z. Xu, J. Xia, S. T. Tsai, Y. Wu, G. Li, C. Ray L. Yu, *Adv. Mater.* **2010**, *22*, E135–E138; (d) H. Y. Chen, J. Hou, S. Zhang, Y. Liang, G. Yang, Y. Yang, L. Yu, Y. Wu, G. Li, *Nat. Mater.* **2007**, *6*, 497–500.

28 T. K. An, S. M. Park, S. Nam, J. Hwang, S. J. Yoo, M. J. Lee, W. M. Yun, J. Jang, H. Cha, J. Hwang, S. Park, J. Kim, D. S. Chung, Y. H. Kim, S. K. Kwon, C. E. Park, *Sci. Adv. Mater.* **2013**, *5*, 1323–1327.

29 (a) J. K. Lee, W. L. Ma, C. J. Brabec, J. Yuen, J. S. Moon, J. Y. Kim, K. Lee, G. C. Bazan, A. J. Heeger, *J. Am. Chem. Soc.* **2008**, *130*, 3619–3623; (b) T. Salim, L. H. Wong, B. Bräuer, R. Kukreja, Y. L. Foo, Z. Bao, Y. M. Lam, *J. Mater. Chem.* **2011**, *21*, 242250; (c) Y. Yao, J. Hou, Z. Xu, G. Li, Y. Yang, *Adv. Funct. Mater.* **2008**, *18*, 1783–1789; (d) C. H. Hsieh, Y. J. Cheng, P. J. Li, C. H. Chen, M. Dubosc, R. M. Liang, C. S. Hsu, *J. Am. Chem. Soc.* **2010**, *132*, 4887–4893; (e) J. S. Moon, C. J. Takacs, S. Cho, R. C. Coffin, H.; Kim, G. C. Bazan, A. J. Heeger, *Nano Lett.* **2010**, *10*, 4005–4008; (f) J. T. Rogers, K. Schmidt, M. F. Toney, E. J. Kramer G. C. Bazan, *Adv. Mater.* **2011**, *23*, 2284–2288; (g) C. Liu, X. Hu, C. Zhong, M. Huang, K. Wang, Z. Zhang, X. Gong, Y. Cao, A. J. Heeger, *Nanoscale* **2014**, *6*, 14297–14304.

30 (a) D. Di Nuzzo, A. Aguirre, M. Shahid, V. S. Gevaerts, S. C. J. Meskers, R. A. J. Janssen, *Adv. Mater.* **2010**, *22*, 4321; (b) W. W. Li, Y. Zhou, B. V. Andersson, L. M. Andersson, Y. Thomann, C. Veit, K. Tvingstedt, R. P. Qin, Z. S. Bo, O. Inganas, U. Wurfel, F. L. Zhang, *Org. Electron.* **2011**, *12*, 1544.

31 H. Cha, J. Y. Baek, T. K. An, S. O. Kim, S. K. Kwon, Y. H. Kim C. E. Park, *Org. Electron.* **2014**, *15*, 3558–3567.

32 R. A. Janssen, J. R. Nelson, *Adv. Mater.* **2013**, *25*, 1847–1858.

33 L. Lu, T. Xu, W; Chen, J. M. Lee, Z. Luo, I. H. Jung, H. I. Park, S. O. Kim, L. Yu, *Nano Lett.* **2013**, *13*, 2365–2369.

34 (a) F. Zhang, Z. Zhuo, J. Zhang, X. Wang, X. Xu, Z. Wang, Y. Xin, J. Wang, J. Wang, W. Tang, *Sol. Energy Mater. Sol. Cells* **2012**, *97*, 71–77; (b) D. Huang, Y. Li, Z. Xu, S. Zhao, L. Zhao, J. Zhao, *Phys. Chem. Chem. Phys.* **2015**, *17*, 8053–8060.

35 (a) T. Y. Chu, O. K. Song, *Appl. Phys. Lett.* **2007**, *90*, 203512; (b) J. Huang, Y. Zhao, W. He, H. Jia, Z. Lu, B. Jiang, C. Zhan, Q. Pei, Y. Liu, J. Yao, *Polym. Chem.* **2012**, *3*, 2832–2841; (c) G. G. Malliaras, J. R. Salem, P. J. Brock, C. Scott, *Phys. Rev. B* **1998**, *58*, 13411; (d) P. W. M. Blom, M. J. M. de Jong, M. G. van Munster, *Phys. Rev. B* **1997**, *55*, R656.

36 (a) Z. Wang, F. Zhang, L. Li, Q. An, J. Wang, J. Zhang, *Appl. Surf. Sci.* **2014**, *305*, 221–226; (b) J. Wang, F. Zhang, L. Li, Q. An, J. Zhang, W. Tang F. Teng, *Sol. Energy Mater. Sol. Cells* **2014**, *130*, 15–19.

37 (a) P. Schilinsky, C. Waldauf, C. J. Brabec, *Appl. Phys. Lett.* **2002**, *81*, 3885–3887; (b) J. K. J. van Duren, X. Yang, J. Loos, C. W. T. Bulle-Lieuwma, A. B. Sieval, J. C. Hummelen, R. A. J. Janssen, *Adv. Funct. Mater.* **2004**, *14*, 425–434.